

Can EDGES observation favour any dark matter model?

A. Rudakovskiy,^{1,2}★ D. Savchenko,^{1,2} M. Tsizh³

¹*Bogolyubov Institute for Theoretical Physics of the NAS of Ukraine, Metrolohichna Str. 14-b, Kyiv, 03143, Ukraine*

²*Kyiv Academic University, 36 Vernadskyi blvd., Kyiv, 03142, Ukraine*

³*Astronomical Observatory of Ivan Franko National University of Lviv, Kyryla i Methodia Str., 8, Lviv 79005, Ukraine*

Accepted XXX. Received YYY; in original form ZZZ

ABSTRACT

The recent detection of the 21-cm absorption signal by the EDGES collaboration has been widely used to constrain the basic properties of dark matter particles. However, extracting the parameters of the 21-cm absorption signal relies on a chosen parametrization of the foreground radio emission. Recently, the new parametrizations of the foreground and systematics have been proposed, showing significant deviations of the 21-cm signal parameters from those assumed by the original EDGES paper. In this paper, we consider this new uncertainty, comparing the observed signal with the predictions of several dark matter models, including the widely used cold dark matter model, 1–3 keV warm dark matter models, and 7 keV sterile neutrino (SN7) model, capable of producing the reported 3.5 keV line. We show that all these dark matter models cannot be statistically distinguished using the available EDGES data.

Key words: cosmology: cosmic background radiation – cosmology: observations – cosmology: dark ages, reionization, first stars – cosmology: dark matter

1 INTRODUCTION

The possibility of observation of the cosmological 21-cm hydrogen signal was of interest to cosmologists even before the first observational constraints became real (see e.g. Hogan & Rees 1979; Scott & Rees 1990; Madau et al. 1997). There are two possible ways in which this observation may shed light on the structure formation processes in the early Universe. The first one is the 21-cm tomography, which is based on the study of the spatial distribution of fluctuations of the 21-cm signal generated by HI clouds at the Dark Ages and reionization epochs (see e.g. Madau et al. 1997; Ciardi & Ferrara 2005; McQuinn et al. 2006; Mao et al. 2008; Morales & Wyithe 2010). The second one is the detection of the sky-averaged signal from the Dark Ages epoch (see e.g. Mirocha et al. 2013; Mirocha et al. 2015; Cohen et al. 2017) produced by absorption of the cosmic microwave background (CMB) radiation by the neutral hydrogen. This absorption is caused by the Wouthuysen–Field coupling between the spin temperature of hydrogen and Ly α radiation of the first galaxies. For a detailed description of the theoretical and observational challenges of 21-cm signal detection, (see e.g. Furlanetto et al. 2006; Pritchard & Loeb 2008; Pritchard & Loeb 2012, and references therein).

Detection of the global absorption signal claimed by the EDGES collaboration (Bowman et al. 2018) caused great excitement among physicists. While the central frequency of the absorption peak (which is linked to the redshift at which it was generated) is in a good agreement with the predictions of the Lambda-CDM

model (Cohen et al. 2017),¹ the amplitude (~ 0.5 K) of the observed signal appears to be at least twice that of the most extreme absorption predicted in the Lambda-CDM model (see e.g. Cohen et al. 2017).

Observation of the global 21-cm absorption by EDGES motivated a wide search of possible mechanisms that would explain the observed depth and position of the absorption signal. This opened up a possibility to study and put constraints on the early star formation rate (see e.g. Madau 2018; Schauer et al. 2019), structure formation in dark matter models (Safarzadeh et al. 2018; Schneider 2018; Chatterjee et al. 2019; Boyarsky et al. 2019b; Leo et al. 2020) and non-standard X-ray sources that can heat the IGM such as the first black holes (Clark et al. 2018) and decaying or annihilating dark matter (Mitridate & Podo 2018; Cheung et al. 2019; Liu & Slatyer 2018; Yang 2018; D’Amico et al. 2018; Fraser et al. 2018; Hektor et al. 2018; Clark et al. 2018; Chatterjee et al. 2019; Chianese et al. 2019). Additional mechanisms beyond the standard cosmological scenario were proposed to explain the depth of the absorption signal, such as the interaction between baryonic matter and dark matter (Barkana 2018; Fialkov et al. 2018; Bhatt et al. 2019) and extreme radio background during the Dark Ages (Feng & Holder 2018; Ewall-Wice et al. 2018; Fialkov & Barkana 2019), alternative dark energy models (Hill & Baxter 2018; Li et al. 2020; Yang et al. 2019).

¹ However, explanation of the frequency of absorption feature reported by EDGES requires more efficient star formation in low-mass galaxies compared to that extrapolated from $z \sim 6-8$; see more in (Mirocha & Furlanetto 2019).

★ E-mail: rudakovskiy@bitp.kiev.ua

At the same time, a well-known problem of detecting the 21-cm signal is that the galactic synchrotron emission and ionospheric emission and absorption are dominant over the signal by four orders of magnitude at frequencies below 100 MHz (Bernardi et al. 2015). Therefore, it is not surprising that soon after the EDGES publication several works appeared addressing the technical details of extracting the 21-cm signal from the observation and questioning the reliability and validity of the observed profile. Hills et al. (2018) reanalysed the data reported by EDGES. They showed that the original analysis assumed a controversial structure in the spectrum of the foreground (galactic) emission in the studied spectral band and led to non-physical properties of the ionosphere. Bradley et al. (2019) reported a possible systematic artefact in the observations that can affect the determination of the absorption signal.

The 21-cm signal naturally depends on structure formation history. In turn this history depends on the underlying dark matter model. Unlike the standard CDM scenario, in warm dark matter (WDM) models particles have masses of the order of few keV and relativistic initial velocities. This fact leads to the smearing of density perturbations on scales below the free-streaming length λ_{fs} (Boyarsky et al. 2009, 2019a) and suppression of the structure formation on such small scales, compared to the predictions of CDM. The WDM particle candidates naturally arise in some extensions of the Standard Model [gravitino (see e.g. Viel et al. 2005), sterile neutrino (see e.g. Boyarsky et al. 2019a, and references therein) etc.]. The warm dark matter particles may reach thermal equilibrium with other particles (gravitinos) or have non-equilibrium distribution (sterile neutrinos). The lack of the small-scale structures in the warm dark matter scenario could modify the position and the form of the 21-cm signal in comparison with CDM (see e.g. Sitwell et al. 2014). The main goal of this manuscript is a study of the possibility to distinguish between warm and cold DM models via the ‘raw’ EDGES data.

This work has the following plan. In the next section we describe how we use the foreground modelling proposed in (Hills et al. 2018) and take into account the ground plane artefact discussed in (Bradley et al. 2019) to best fit the EDGES data via the non-linear least-squares procedure. Next, we model the 21-cm global signal with the ARES code for different models of dark matter [CDM, thermal relic WDM and 7 keV sterile neutrino decaying dark matter motivated by the recently detected 3.5 keV line (Boyarsky et al. 2014; Bulbul et al. 2014; Boyarsky et al. 2018)²]. Then, in the *Results* section we fit the EDGES data subtracting the obtained different absorption signals and compare the fitting scores in order to select the preferred dark matter model. In the last, *Conclusions and Discussion* section we briefly summarize our results and discuss the possibility to constrain the parameters of structure formation during the Dark Ages and, in particular, dark matter properties by the EDGES data and by the planned observations of 21-cm absorption signal.

2 METHODS

2.1 Fitting the EDGES data

We represent the EDGES data with a sum of three components,

$$T(\nu) = T_{\text{sky}}(\nu) + T_{\text{res}}(\nu) + T_{21}(\nu). \quad (1)$$

² Such dark matter is in a good agreement with the Ly α forest analysis (Baur et al. 2017) and reionization history data (Rudakovskiy & Iakubovskiy 2019).

Here, the first term is the sky foreground brightness temperature. In the original EDGES paper (Bowman et al. 2018), this foreground was modelled in the linearized form. However, (Hills et al. 2018) argued that the parameters of such a representation assume non-physical values in the best-fitting model. In our fits, we used the non-linear model with the ionospheric absorption and emission terms being connected through the electronic temperature T_e , obtained by expanding the foreground temperature around some central frequency ν_c as described in (Hills et al. 2018):

$$T_{\text{sky}}^{\text{H18}}(\nu) = b_0 \left(\frac{\nu}{\nu_c} \right)^{-2.5+b_1+b_2 \ln(\nu/\nu_c)} e^{-b_3(\nu/\nu_c)^{-2}} + T_e \left(1 - e^{-b_3(\nu/\nu_c)^{-2}} \right). \quad (2)$$

Here, the electronic temperature T_e is allowed to vary in the range [200, 2000] K, according to the EDGES measurements, see fig. 2 of (Rogers et al. 2015). The parameter b_1 is a correction to the overall power-law index, which varies by ~ 0.1 across the sky according to (Bowman et al. 2018). In our fits we allow this parameter to vary in a broader range of $[-0.2, 0.2]$. The parameter b_2 was left unconstrained, although its best-fitting value should be controlled to be ~ 0.1 according to (Bernardi et al. 2015). The ionospheric opacity b_3 is allowed to vary between 0 and 0.03 according to (Hills et al. 2018).

The second term in equation (1) is the sum of three resonant absorption components described in (Bradley et al. 2019):

$$T_{\text{res}}(\nu) = - \sum_{i=1}^3 \frac{A_i \nu^3 \nu_{0i}}{\nu^4 + Q_i^2 (\nu^2 - \nu_{0i}^2)^2}. \quad (3)$$

This term is characterized by three parameters: the central frequencies ν_{0i} , the depths of the profiles $A_i \equiv A(\nu_{0i})$, and the quality factors Q_i which are the ratios of ν_{0i} to the spectral widths of absorption. The phenomenological origin of this term is the fact that soil itself is a resonator, of which one cannot get rid. EDGES uses the ground antennae, and possible discontinuities at the edges of the ground plate produce resonant features and distort the signal.

The last term in equation (1), $T_{21}(\nu)$, is the global 21-cm absorption signal. While (Bowman et al. 2018) modelled it in the form of flattened Gaussian, we do not represent it in any analytical form. Instead, from the initial EDGES data we subtract the absorption profile obtained in the ARES simulation, taking into account the specific structure formation model, which includes the influence from the particular type of the halo mass function and DM decays (see Sec. 2.2).

The EDGES data do not include error bars. Therefore, we use the two following approaches for analysis of the EDGES data. According to the first one, we follow Bradley et al. (2019) and choose the objective function in the form of the minimal log likelihood $-\ln L = \frac{1}{2} \sum_{kl} (y_k - \hat{y}_k) C_{kl}^{-1} (y_l - \hat{y}_l)$ with the noise covariance matrix $C_{kl} \propto y_k^2 \delta_{kl}$, where y_i are the data points and \hat{y}_i are the model values. The constant of proportionality is not defined; however, it changes only the magnitude of the log-likelihood as function of parameters, not the shape, allowing to produce a weighted fit. As a result of the fitting procedure, the root mean square (rms) score could be calculated for the best-fitting parameters. Due to the undefined absolute values of the errors, we cannot use the standard chi-squared test to quantify the differences in the goodness-of-fits between models.

Therefore, in the second approach we follow the logic of Singh & Subrahmanyam (2019) and assume the error bars to be the same for all data points. The covariance matrix has the form $C_{kl} = c_k \delta_{kl}$

here, with the constant of proportionality c_k being also unknown. This leads to the unweighted least-squares fitting procedure. In such case, we can use the Bayesian information criterion (BIC) for model selection. For the uniform Gaussian errors it could be written as (Schwarz 1978; Priestley 1983)

$$\text{BIC} = N \ln \left(\frac{1}{N} \sum_{i=1}^N (y_i - \hat{y}_i)^2 \right) + k \ln N. \quad (4)$$

Here, y_i denotes the data points and \hat{y}_i are the model values, N is the number of the data points ($N = 123$ for the EDGES data), and k is the number of free model parameters ($k = 15$ for our model). Notice that the extraction of the simulated signal from the raw spectra does not change the values of N and k . The model with the lower BIC could be treated as strongly preferred if the difference between BICs is higher than 6, and one cannot talk of any preference for $\Delta\text{BIC} < 2$ (Kass & Raftery 1995).

In both case, we use the non-linear least-squares procedure implemented in the `lmfit` PYTHON package (Newville et al. 2018). Because the underlying Levenberg–Marquardt algorithm depends on the initial guess for the parameters, we repeat fits many times, randomly varying these initial values and select the fit with the highest likelihood.

2.2 Modelling the global 21-cm absorption profile

We use the open-sourced Accelerated Reionization Era Simulations (ARES) code (Mirocha 2014; Mirocha et al. 2017; Mirocha & Furlanetto 2019) to compute the global 21-cm neutral hydrogen signal in different DM models. This code produces the profile of the global 21-cm signal for given star formation rate, halo mass function and cosmology. The PopII stars in the galaxies are assumed to be the sources of the Ly α and ionizing UV-radiation, and black holes produce X-rays. Also, there is a possibility to add new sources of radiation, like, for example, decaying DM.

We adopt the cosmological parameters defined by Planck Collaboration (2016), namely $\Omega_\Lambda = 0.685$, $\Omega_m = 0.315$, $\Omega_b = 0.049$, $h = 0.673$, $n_s = 0.965$, and $\sigma_8 = 0.83$.

The halo abundance is usually described by the halo mass function:

$$\frac{dn}{d\ln M} = f(x) \frac{\bar{\rho}_m}{M} \frac{d\ln \sigma^{-1}}{d\ln M}, \quad (5)$$

where $x = \left(\frac{\delta_c^2(z)}{\sigma^2} \right)$, $\delta_c(z) = \frac{1.686}{D(z)}$, $D(z)$ is the growth factor (Heath 1977), $\sigma(M)$ is the variance of the density fluctuations on the mass scale M , and $\bar{\rho}_m$ is the mean matter density of the Universe.

We use the results of the N -body simulations for thermal relic WDM and CDM scenarios at high redshifts from Schneider (2018) as a reference for our halo mass function fitting formula. Following Schneider (2018) for all DM models, we use the Sheth–Tormen approximation (Sheth & Tormen 2002):

$$f(x) = A_{ST} \sqrt{\frac{2qx}{\pi}} (1 + (qx)^{-p}) e^{-qx/2}. \quad (6)$$

We find that the parameters $A_{ST} = 0.322$, $q = 0.93$, and $p = 0.3$ are in a best agreement with the CDM and WDM simulations, shown in fig.1 of (Schneider 2018)³.

³ Note that in Schneider (2018) the parameter q is claimed to be equal to 1. However, we found that $q = 0.93$ is the best-fitting parameter value for the simulation points provided in Schneider (2018).

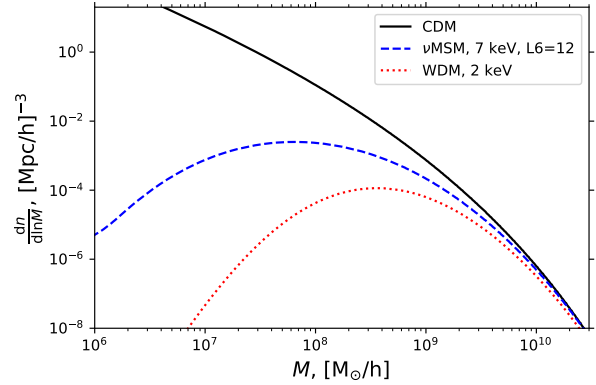


Figure 1. Halo mass functions for CDM, WDM with particle mass $m = 2$ keV, and 7 keV sterile neutrino with $L_6 = 12$ at $z = 17$.

Following Schneider (2018), we also consider a sharp- k filter for $\sigma(M)$ calculation, which provides a good fit for the CDM and WDM halo mass functions, obtained during N -body simulations at different redshifts (Benson et al. 2013; Schneider 2015, 2018): $\sigma^2 = \int_0^{k_c} P(k) \frac{d^3k}{(2\pi)^3}$, where $P(k)$ is the dark matter power spectrum, which depends on the properties of the DM particles. The mass of the halo and k_c are related as $M = \frac{4\pi}{3} \bar{\rho}_m \left(\frac{2.5}{k_c} \right)^3$.

Warm dark matter power spectrum can be connected with cold dark matter power spectrum $P_{\text{CDM}}(k)$ as: $P_{\text{WDM}}(k) = P_{\text{CDM}} T^2(k)$, where $T(k)$ is the so-called transfer function. For transfer functions of WDM in the form of thermal relic (e.g. gravitino), we adopt the fitting formula by Viel et al. (2005):

$$T(k) = (1 + (\alpha k)^{2\nu})^{-5/\nu}, \quad (7)$$

where

$$\alpha = 0.049 \left(\frac{m}{1 \text{ keV}} \right)^{-1.11} \left(\frac{\Omega_{\text{WDM}}}{0.25} \right)^{0.11} \left(\frac{h}{0.7} \right)^{1.22} h^{-1} \text{ Mpc}, \quad (8)$$

$\Omega_{\text{WDM}} = \Omega_{\text{DM}}$, $\nu = 1.12$, m is the mass of thermal relic WDM particle.

While in WDM models in the form of thermal relic the free-streaming length and power spectrum depend only on the particle mass, for sterile neutrino they also depend on the production mechanism. We use power spectrum for the 7 keV sterile neutrino, generated with the lepton asymmetry $L_6 = 12$ (Lovell et al. 2016, 2017).

For each of the DM models under consideration, we generate the corresponding halo mass functions for redshifts z between 0 and 50. For thermal relic WDM and CDM we use the `hmf` public code (Murray et al. 2013). Examples of such halo mass functions at $z = 17$ are shown in Fig. 1.

The star formation rate density (SFRD) is modelled by the standard so-called `fcoll` model used in ARES:

$$\dot{\rho}_* = f_* \rho_b \frac{d}{dt} f_{\text{coll}}(z). \quad (9)$$

The star formation efficiency f_* in our analysis is considered, for simplicity, to be a constant not exceeding unity. The constant star formation efficiency is different from the default ARES parametrization of f_* by a double-power-law function of the halo mass (Mirocha et al. 2017). The plausibility of our assumption is motivated by the fact that the star formation efficiency is unknown at high redshifts,

and by a degeneracy between the effects of mass of the particle of warm dark matter and f_* (Sitwell et al. 2014; Boyarsky et al. 2019b, see e.g.). The collapsed fraction f_{coll} is defined as

$$f_{\text{coll}}(z) = \frac{1}{\rho_m} \int_{M_{\text{min}}}^{\infty} \frac{dn}{d \ln M} dM, \quad (10)$$

where M_{min} is the minimal mass of the source, determined by the virial temperature T_{vir} , similarly to (Barkana & Loeb 2001). In this work we assume that $T_{\text{vir}} = 10^4 K$. The specific emissivity in a particular spectral band between E_{min} and E_{max} is proportional to *SFRD* (see e.g. Mirocha 2014):

$$\epsilon(E, z) = c \dot{\rho}_*(z) I(E), \quad (11)$$

where c is the conversion factor between emissivity and *SFRD*, and $I(E)$ is the spectral density normalized as $\int_{E_{\text{min}}}^{E_{\text{max}}} I(E) dE = 1$.

Throughout this work, we assume the default ARES parameters (except for f_*) for the Ly α and Ly C photons produced by PopII stars in the first galaxies and X-rays generated by the accretion of baryonic matter onto the first black holes.

Another possible source of X-ray photons are decaying DM particles. The recently detected narrow 3.5 keV line in the spectra of the DM dominated objects (Boyarsky et al. 2014, 2015; Bulbul et al. 2014) may be emitted during the DM decay. One of the best-motivated DM candidates, which might explain the 3.5 keV line, is ~ 7 keV sterile neutrino (see e.g. Adhikari et al. 2017; Boyarsky et al. 2019a, and references therein). We focus on the resonantly produced 7 keV sterile neutrino DM with the lepton asymmetry $L_6 = 12$, corresponding to the mixing angle $\sin^2 2\theta = 1.6 \times 10^{-11}$ according to (Lovell et al. 2016), and lifetime $\tau_{\text{DM}} = 2.677 \times 10^{28}$ s consistent with Boyarsky et al. (2018). We model the dark matter decays in ARES as a new population similar to black holes with constant accretion rate. For decaying DM models (including the model of 7 keV sterile neutrino), the luminosity density of photons with energy E_γ generated via decays is

$$L_{\text{decays}} = E_\gamma \frac{\rho_{\text{DM}}}{m_{\text{DM}}} \frac{1}{\tau_{\text{DM}}}. \quad (12)$$

3 RESULTS

First, we basically reproduce the modelling by (Bowman et al. 2018) and (Bradley et al. 2019) to justify our fitting method (see Appendices A and B).

Then we generate the absorption signals for the different dark matter models (CDM; 1, 2, and 3 keV thermal relic WDM, 7 keV decaying sterile neutrinos), each with different values of f_* in the range from 0.01 to 1, while all other astrophysical and cosmological parameters are fixed. We subtract these signals from the data and perform the fits as described in Sec. 2.1.

The minimal rms in the weighted least-square procedure is obtained for the 3 keV WDM model with $f_* = 0.52$ and is equal to 20.72 mK and the maximal rms is 20.9 mK in the 2 keV WDM model with $f_* = 0.8$. All these values are close to 20.8 mK obtained in (Bradley et al. 2019) and better than 25 mK from (Bowman et al. 2018). However, one cannot draw robust conclusions about the difference in the fitting qualities between these models due to the different number of free parameters in models.

In the unweighted least-square approach, the obtained rms for all DM models and all f_* are in the range of 20.66 – 20.72 mK, which correspond to BICs in the range of –881.47 to –882.20 for

$k = 15$ and $N = 123$. Thereby, differences in the values of BICs are all below 2, so we conclude that all tested dark matter particle models are indistinguishable.

Examples of specially interesting cases (standard CDM and decaying sterile neutrino dark matter) are shown in Figs. 2 and 3.

We also test the case without any absorption signal at all. In the weighted least-squares procedure the obtained rms is 20.87 mK. In the unweighted approach the rms is 20.7 mK, which corresponds to $\text{BIC} = -881.7$, showing that the absence of a signal is also allowed by the data.

Additionally, we perform unweighted least-square fits with the foreground model alone, not including the instrumental resonant components (number of parameters $k = 6$). Subtracting signals, corresponding to the CDM and 2 keV WDM, we find, that the best-fitting rms is 0.215 mK, corresponding to $\text{BIC} = -349.09$. Moreover, residuals have a clearly visible oscillating feature. This shows that foreground-only model is strongly disfavoured.

We have performed the same computations with Planck-18 cosmological parameters (Planck Collaboration 2018). In such case, the calculated rms and BICs appear to be very close to the results, obtained in Planck-15 cosmology.

4 CONCLUSIONS AND DISCUSSION

We have modelled the EDGES data with the alternative to (Bowman et al. 2018) physically motivated foreground model proposed by Hills et al. (2018), taking into account the ground plane artefact absorption by Bradley et al. (2019), and subtracting different simulated 21-cm absorption profiles in order to constrain the underlying dark matter model. We have explicitly shown that the fit quality of such model does not depend on the assumed dark matter particle model, concluding that the EDGES observation cannot be used as a good tool for the quantitative constraining of dark matter particle models. Moreover, one cannot even distinguish between existence or absence of a signal.

Unlike the papers in which the form and position of the signal reported by (Bowman et al. 2018) are used to constrain the dark matter models (see e.g. Safarzadeh et al. 2018; Schneider 2018; Clark et al. 2018; Hektor et al. 2018; Chatterjee et al. 2019), our paper uses the ‘raw’ signal $T(\nu)$ to perform the modelling.

(Bradley et al. 2019) proposed a physically motivated instrumental feature; however, one can try to check other forms of systematics. For example, (Singh & Subrahmanyan 2019) showed that the EDGES spectrum is consistent with the standard cosmology if the maximally smooth polynomial foreground and sinusoidal systematics are assumed. Their fit gives $\text{BIC} = -894.2$, formally strongly preferred over our best value of –882.2. It is a matter of choosing the form of the foreground and of the term describing the systematics. This brings in uncertainty and model dependence into the exploration of the global absorption signal. Moreover, the global 21-cm signal is averaged over the sky and contains contributions from many different sources; thus no simple physical model may be appropriate to fit it.

Sims & Pober (2020) also make direct fitting of EDGES data considering ARES simulations of the 21-cm signal and use the oscillating form of systematics. Direct parametrization of the noise covariance matrix allows them to explicitly evaluate the log(evidence) in the weighted fitting procedure. However, only standard cold dark matter scenario have been considered.

The developed radiometer experiments such as BIGHORNS (Sokolowski et al. 2015), SARAS 2 (Singh et al. 2018), and LEDA

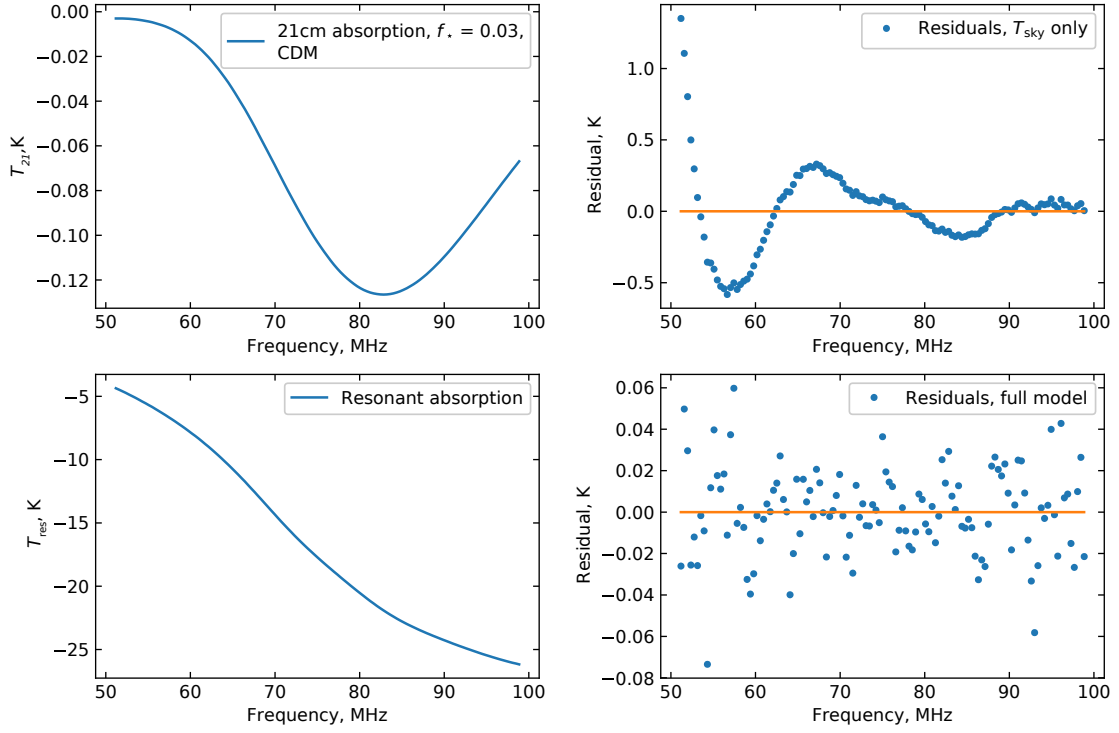


Figure 2. Results of the weighted fits, assuming the 21-cm absorption in the CDM model with $f_{\star} = 0.03$. *Top left:* Absorption profile in the frequency range where the fit is performed. *Top right:* Residuals after fitting and removing only the foreground model, equation (2). *Bottom left:* The best-fitting model of the instrumental resonant absorption feature, equation (3). *Bottom right:* Residuals after removing both the foreground and the resonant absorption model.

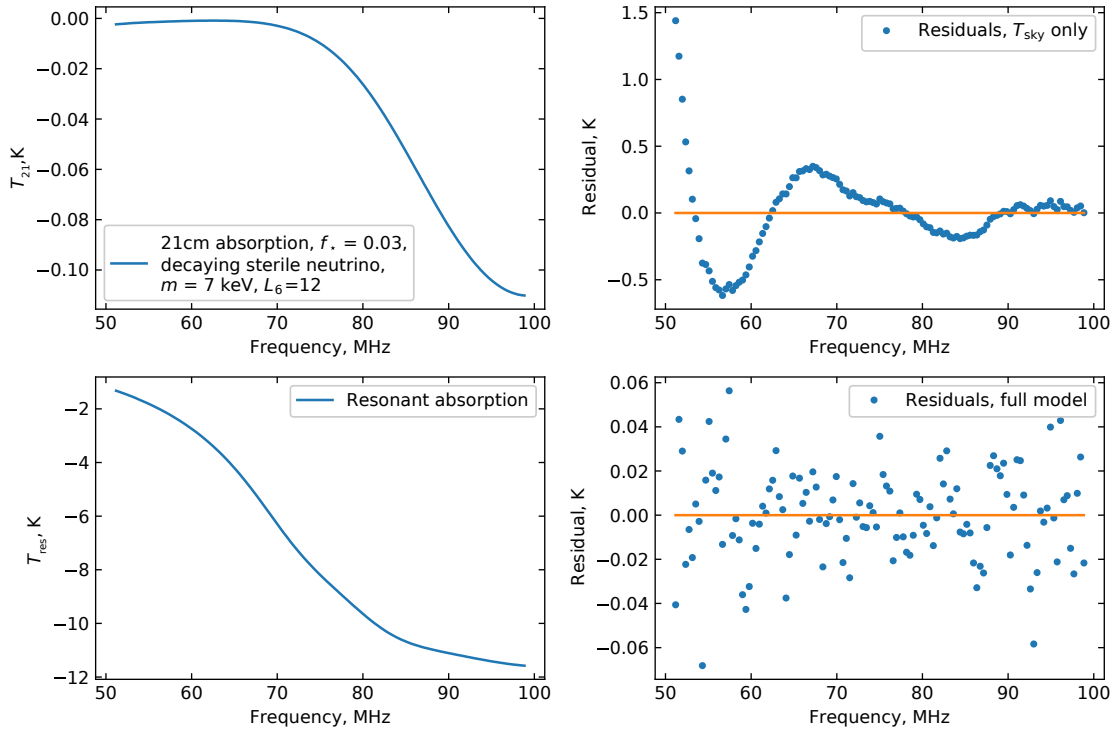


Figure 3. The same as in Fig. 2, but assuming the 21-cm absorption in the 7 keV sterile neutrino dark matter model with $f_{\star} = 0.03$.

(Price et al. 2018), which will be focused on the global 21-cm signal, may shed new light on the 21-cm absorption feature. However, there are large uncertainties in the star formation in galaxies during the reionization and Dark Ages epochs, which makes it difficult to constrain a dark matter scenario by using the global 21-cm absorption signal (Boyarsky et al. 2019b). Nevertheless, the future studies of the statistics of the spatial distribution of the 21-cm signal by radio interferometers such as MWA, HERA and SKA may help to break the degeneracy between the baryonic and dark matter effects during the reionization and Dark Ages epochs (see e.g. Mesinger et al. 2014; Sitwell et al. 2014; Weltman et al. 2020).

ACKNOWLEDGEMENTS

The authors are grateful to Dr. D. Iakubovskiy and Dr. G. Sun for valuable comments and to Prof. Dr. Yu. Shtanov for reading and commenting on this paper. We thank the anonymous referee for the comments that significantly improved the quality of the paper. This work was supported by the grant for young scientist research laboratories of the National Academy of Sciences of Ukraine. The work of A.R. was also partially supported by the ICTP through AF-06.

APPENDIX A: REPRODUCING THE ORIGINAL EDGES RESULTS

In the original EDGES paper (Bowman et al. 2018), the foreground was modelled as

$$T_{\text{sky}}^{(\text{B18})}(\nu) = a_0 \left(\frac{\nu}{\nu_c} \right)^{-2.5} + a_1 \left(\frac{\nu}{\nu_c} \right)^{-2.5} \ln \left(\frac{\nu}{\nu_c} \right) + a_2 \left(\frac{\nu}{\nu_c} \right)^{-2.5} \left[\ln \left(\frac{\nu}{\nu_c} \right) \right]^2 + a_3 \left(\frac{\nu}{\nu_c} \right)^{-4.5} + a_4 \left(\frac{\nu}{\nu_c} \right)^{-2}. \quad (\text{A1})$$

The absorption signal was assumed in the form of a flattened Gaussian:

$$T_{21}^{(\text{B18})}(\nu) = -A \left(\frac{1 - e^{-\tau e^B}}{1 - e^{-\tau}} \right), \quad (\text{A2})$$

where

$$B = \frac{4(\nu - \nu_0)^2}{w^2} \ln \left[-\frac{1}{\tau} \ln \left(\frac{1 + e^{-\tau}}{2} \right) \right], \quad (\text{A3})$$

We fit the data with the sum of the sky foreground brightness temperature in the form of equation (A1), and the 21-cm absorption term in the form of the flattened gaussian, equation (A2).

Our best-fitting model closely reproduces the results reported by the EDGES collaboration. The best-fitting values for the 21-cm model parameters are $A = 0.056$ K, $w = 18.8$ MHz, and $\tau = 5.8$. The resulting rms is 24.5 mK (close to 0.025 K reported by Bowman et al. 2018). The summary of our results is plotted in Fig. A1.

APPENDIX B: REPRODUCING THE ORIGINAL BRADLEY'S RESULTS

We also reproduce the findings by (Bradley et al. 2019) so that the EDGES spectrum can be modelled with a sum of cosmic foreground continuum in the linearized form of equation (A1), taking into account only the first two terms, and three resonant features of the ground plane patch absorber (equation 3). The obtained best root

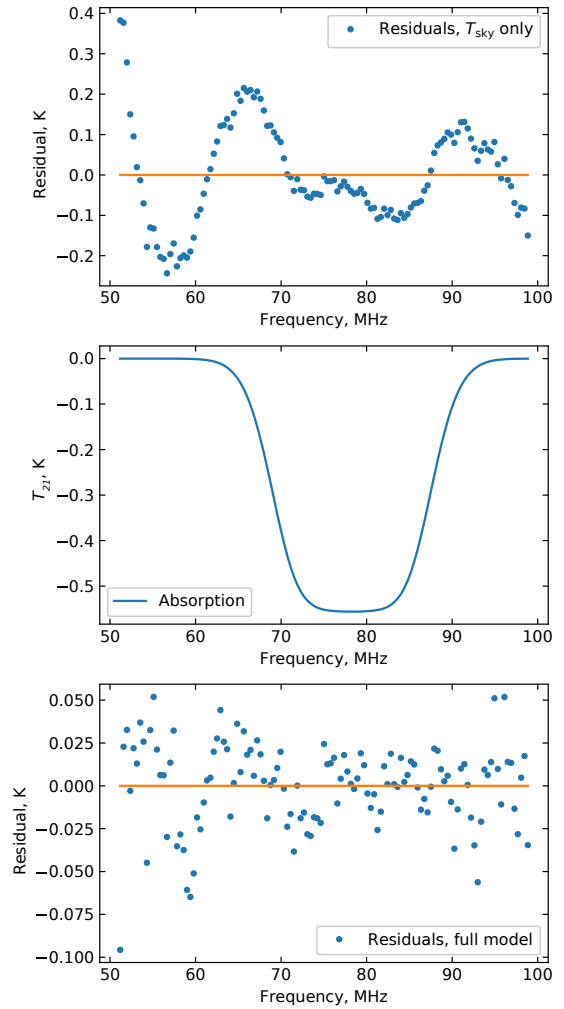


Figure A1. Best-fitting results, reproducing (Bowman et al. 2018). *Top:* Residuals after fitting and removing only the foreground model, equation (A1) (see their fig. 1b). *Middle:* The best-fitting model of the 21-cm absorption feature, equation (A2) (see their fig. 1d). *Bottom:* Residuals after removing both the foreground and the 21-cm absorption model (see their fig. 1c).

mean square residual is 20.8 mK, the same as reported by (Bradley et al. 2019). The resonant absorption profile together with the model residuals are plotted in Fig. B1.

DATA AVAILABILITY

The EDGES low-band spectrum underlying this article is publicly available at: <http://loco.lab.asu.edu/edges/edges-data-release>. The code that supports the findings of this study will be shared on reasonable request to the corresponding author.

REFERENCES

- Adhikari R., et al., 2017, *J. Cosmology Astropart. Phys.*, 2017, 025
 Barkana R., 2018, *Nature*, 555, 71
 Barkana R., Loeb A., 2001, *Phys. Rep.*, 349, 125

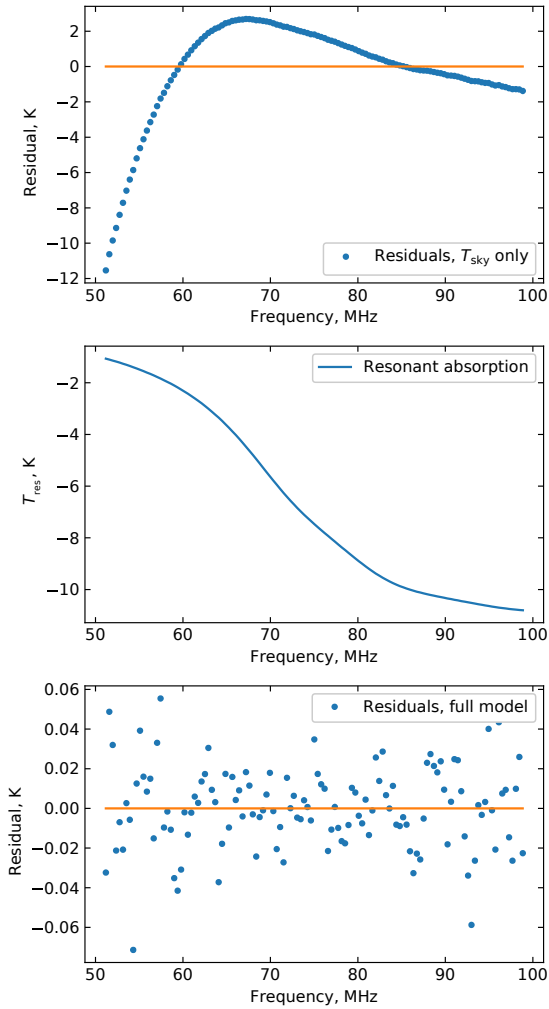


Figure B1. Best-fitting results, reproducing (Bradley et al. 2019). *Top:* Residuals after fitting and removing only the foreground model (first two terms of equation A1). *Middle:* The best-fitting model of the instrumental resonant absorption feature (equation 3). *Bottom:* Residuals after removing both the foreground and the resonant absorption model.

Baur J., Palanke-Delabrouille N., Yèche C., Boyarsky A., Ruchayskiy O., Armengaud E., Lesgourgues J., 2017, *J. Cosmology Astropart. Phys.*, 2017, 013
 Benson A. J., et al., 2013, *MNRAS*, 428, 1774
 Bernardi G., McQuinn M., Greenhill L. J., 2015, *ApJ*, 799, 90
 Bhatt J. R., Mishra A. K., Nayak A. C., 2019, *Phys. Rev.*, D100, 063539
 Bowman J. D., Rogers A. E. E., Monsalve R. A., Mozdzen T. J., Mahesh N., 2018, *Nature*, 555, 67
 Boyarsky A., Lesgourgues J., Ruchayskiy O., Viel M., 2009, *J. Cosmology Astropart. Phys.*, 2009, 012
 Boyarsky A., Ruchayskiy O., Iakubovskiy D., Franse J., 2014, *Phys. Rev. Lett.*, 113, 251301
 Boyarsky A., Franse J., Iakubovskiy D., Ruchayskiy O., 2015, *Phys. Rev. Lett.*, 115, 161301
 Boyarsky A., Iakubovskiy D., Ruchayskiy O., Savchenko D., 2018, preprint, ([arXiv:1812.10488](https://arxiv.org/abs/1812.10488))
 Boyarsky A., Drewes M., Lasserre T., Mertens S., Ruchayskiy O., 2019a, *Progr. Part. Nucl. Phys.*, 104, 1
 Boyarsky A., Iakubovskiy D., Ruchayskiy O., Rudakovskiy A., Valkenburg W., 2019b, *Phys. Rev.*, D100, 123005
 Bradley R. F., Tauscher K., Rapetti D., Burns J. O., 2019, *ApJ*, 874, 153

Bulbul E., Markevitch M., Foster A., Smith R. K., Loewenstein M., Randall S. W., 2014, *ApJ*, 789, 13
 Chatterjee A., Dayal P., Choudhury T. R., Hutter A., 2019, *MNRAS*, 487, 3560
 Cheung K., Kuo J.-L., Ng K.-W., Tsai Y.-L. S., 2019, *Phys. Lett. B*, 789, 137
 Chianese M., Di Bari P., Farrag K., Samanta R., 2019, *Phys. Lett. B*, 790, 64
 Ciardi B., Ferrara A., 2005, *Space Sci. Rev.*, 116, 625
 Clark S., Dutta B., Gao Y., Ma Y.-Z., Strigari L. E., 2018, *Phys. Rev.*, D98, 043006
 Cohen A., Fialkov A., Barkana R., Lotem M., 2017, *MNRAS*, 472, 1915
 D'Amico G., Panci P., Strumia A., 2018, *Phys. Rev. Lett.*, 121, 011103
 Ewall-Wice A., Chang T.-C., Lazio J., Doré O., Seiffert M., Monsalve R. A., 2018, *ApJ*, 868, 63
 Feng C., Holder G., 2018, *ApJ*, 858, L17
 Fialkov A., Barkana R., 2019, *MNRAS*, 486, 1763
 Fialkov A., Barkana R., Cohen A., 2018, *Phys. Rev. Lett.*, 121, 011101
 Fraser S., et al., 2018, *Phys. Lett.*, B785, 159
 Furlanetto S. R., Oh S. P., Briggs F. H., 2006, *Phys. Rep.*, 433, 181
 Heath D. J., 1977, *MNRAS*, 179, 351
 Hektor A., Hütsi G., Marzola L., Vaskonen V., 2018, *Phys. Lett. B*, 785, 429
 Hill J. C., Baxter E. J., 2018, *J. Cosmology Astropart. Phys.*, 2018, 037
 Hills R., Kulkarni G., Meerburg P. D., Puchwein E., 2018, *Nature*, 564, E32
 Hogan C. J., Rees M. J., 1979, *MNRAS*, 188, 791
 Kass R. E., Raftery A. E., 1995, *J. Am. Stat. Assoc.*, 90, 773
 Leo M., Theuns T., Baugh C. M., Li B., Pascoli S., 2020, *J. Cosmology Astropart. Phys.*, 04
 Li C., Ren X., Khurshudyan M., Cai Y.-F., 2020, *Phys. Lett. B*, B801, 135141
 Liu H., Slatyer T. R., 2018, *Phys. Rev.*, D98, 023501
 Lovell M. R., et al., 2016, *MNRAS*, 461, 60
 Lovell M. R., et al., 2017, *MNRAS*, 468, 4285
 Madau P., 2018, *MNRAS*, 480, L43
 Madau P., Meiksin A., Rees M. J., 1997, *ApJ*, 475, 429
 Mao Y., Tegmark M., McQuinn M., Zaldarriaga M., Zahn O., 2008, *Phys. Rev.*, D78, 023529
 McQuinn M., Zahn O., Zaldarriaga M., Hernquist L., Furlanetto S. R., 2006, *ApJ*, 653, 815
 Mesinger A., Ewall-Wice A., Hewitt J., 2014, *MNRAS*, 439, 3262
 Mirocha J., 2014, *MNRAS*, 443, 1211
 Mirocha J., Furlanetto S. R., 2019, *MNRAS*, 483, 1980
 Mirocha J., Harker G. J. A., Burns J. O., 2013, *ApJ*, 777, 118
 Mirocha J., Harker G. J. A., Burns J. O., 2015, *ApJ*, 813, 11
 Mirocha J., Furlanetto S. R., Sun G., 2017, *MNRAS*, 464, 1365
 Mitridate A., Podo A., 2018, *J. Cosmology Astropart. Phys.*, 2018, 069
 Morales M. F., Wyithe J. S. B., 2010, *ARA&A*, 48, 127
 Murray S. G., Power C., Robotham A. S. G., 2013, *Astron. Comput.*, 3, 23
 Neville M., et al., 2018, *lmfit/lmfit-py* 0.9.12, [doi:10.5281/zenodo.1699739](https://doi.org/10.5281/zenodo.1699739), <https://doi.org/10.5281/zenodo.1699739>
 Planck Collaboration 2016, *A&A*, 594, A13
 Planck Collaboration 2018, preprint, ([arXiv:1807.06209](https://arxiv.org/abs/1807.06209))
 Price D. C., et al., 2018, *MNRAS*, 478, 4193
 Priestley M., 1983, *Spectral Analysis and Time Series, Two-Volume Set: Volumes I and II. Probability and Mathematical Statistics*, Elsevier Science
 Pritchard J. R., Loeb A., 2008, *Phys. Rev.*, D78, 103511
 Pritchard J. R., Loeb A., 2012, *Rep. Progr. Phys.*, 75, 086901
 Rogers A. E. E., Bowman J. D., Vierinen J., Monsalve R., Mozdzen T., 2015, *Radio Sci.*, 50, 130
 Rudakovskiy A., Iakubovskiy D., 2019, *MNRAS*, 483, 4080
 Safarzadeh M., Scannapieco E., Babul A., 2018, *ApJ*, 859, L18
 Schauer A. T. P., Liu B., Bromm V., 2019, *ApJ*, 877, L5
 Schneider A., 2015, *MNRAS*, 451, 3117
 Schneider A., 2018, *Phys. Rev. D*, 98, 063021
 Schwarz G., 1978, *Ann. Stat.*, 6, 461
 Scott D., Rees M. J., 1990, *MNRAS*, 247, 510
 Sheth R. K., Tormen G., 2002, *MNRAS*, 329, 61
 Sims P. H., Pober J. C., 2020, *MNRAS*, 492, 22

- Singh S., Subrahmanyam R., 2019, [ApJ](#), **880**, 26
- Singh S., Subrahmanyam R., Shankar N. U., Rao M. S., Girish B. S., Raghunathan A., Somashekar R., Srivani K. S., 2018, [Exp. Astron.](#), **45**, 269
- Sitwell M., Mesinger A., Ma Y.-Z., Sigurdson K., 2014, [MNRAS](#), **438**, 2664
- Sokolowski M., et al., 2015, [Publ. Astron. Soc. Australia](#), **32**, e004
- Viel M., Lesgourgues J., Haehnelt M. G., Matarrese S., Riotto A., 2005, [Phys. Rev. D](#), **71**, 063534
- Weltman A., et al., 2020, [Publ. Astron. Soc. Australia](#), **37**, e002
- Yang Y., 2018, [Phys. Rev. D](#), **98**, 103503
- Yang W., Pan S., Vagnozzi S., Di Valentino E., Mota D. F., Capozziello S., 2019, [J. Cosmology Astropart. Phys.](#), **2019**, 044

This paper has been typeset from a \LaTeX file prepared by the author.